An Efficient Iris Recognition Algorithm Using Phase-Based Image Matching

Kazuyuki Miyazawa*, Koichi Ito, Takafumi Aoki

Graduate School of Information Sciences, Tohoku University
Sendai-shi 980-8579, Japan
*E-mail: miyazawa@aoki.ecei.tohoku.ac.jp

Koji Kobayashi, Hiroshi Nakajima

Yamatake Corporation
Isehara-shi 259-1195, Japan

Abstract— A major approach for iris recognition today is to generate feature vectors corresponding to individual iris images and to perform iris matching based on some distance metrics. One of the difficult problems in feature-based iris recognition is that the matching performance is significantly influenced by many parameters in feature extraction process, which may vary depending on environmental factors of image acquisition. This paper presents an efficient algorithm for iris recognition using phase-based image matching. The use of phase components in 2D (two-dimensional) discrete Fourier transforms of iris images makes possible to achieve highly robust iris recognition in a unified fashion with a simple matching algorithm. Experimental evaluation using an iris image database clearly demonstrates an efficient matching performance of the proposed algorithm.

I. Introduction

Biometric authentication has been receiving extensive attention over the past decade with increasing demands in automated personal identification. Among many biometrics techniques, iris recognition is one of the most promising approaches due to its high reliability for personal identification [1], [2].

A major approach for iris recognition today is to generate feature vectors corresponding to individual iris images and to perform iris matching based on some distance metrics [1], [2]. Most of the commercial iris recognition systems implement a famous algorithm using "iriscodes" proposed by Daugman [1]. One of the difficult problems in feature-based iris recognition is that the matching performance is significantly influenced by many parameters in feature extraction process (e.g., spatial position, orientation, center frequencies and size parameters for 2D Gabor filter kernel), which may vary depending on environmental factors of iris image acquisition.

This paper presents an efficient algorithm for iris recognition using phase-based image matching — an image matching technique using the phase components in 2D Discrete Fourier Transforms (DFTs) of given images. The technique has been successfully applied to sub-pixel image registration tasks for computer vision applications [3], [4]. In our previous work [5], on the other hand, we have proposed an efficient fingerprint recognition algorithm using phase-based image matching, which has already been implemented in actual fingerprint verification units [6]. In this paper, we demonstrate that the same technique is highly effective also for iris recognition. The use of phase information makes possible to achieve highly robust iris recognition with a simple matching algorithm (as illustrated in Figure 1). Experimental evaluation using the CASIA iris image database [7] clearly demonstrates an efficient matching performance (EER=0%) of the proposed algorithm.

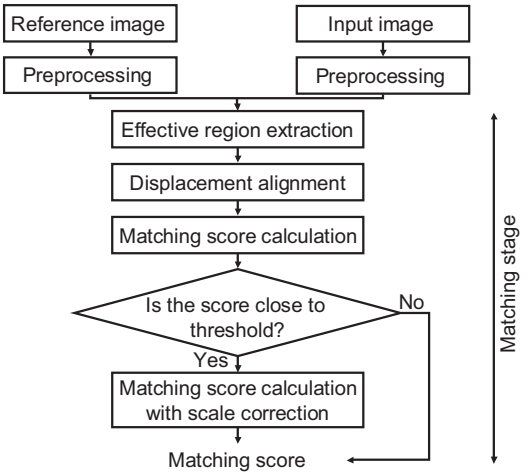

Fig. 1. Flow diagram of the proposed algorithm.

II. Preprocessing

An iris image contains some irrelevant parts (e.g., eyelid, sclera, pupil, etc.). Also, the size of an iris may vary depending on camera-to-eye distance and lighting condition. Therefore, the original image needs to be normalized.

A. Iris Localization

This step is to detect the inner boundary (the boundary between the iris and the pupil) and the outer boundary (the boundary

0-7803-9134-9/05/$20.00 ©2005 IEEE

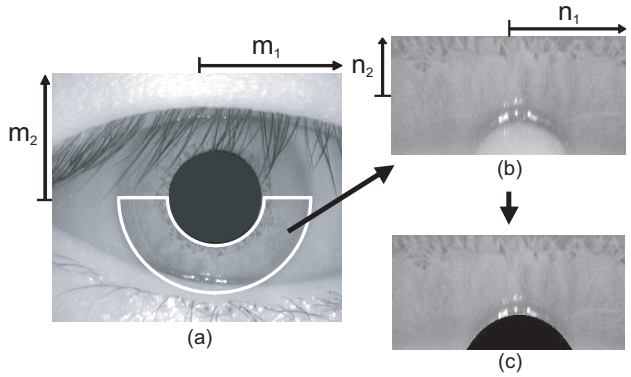

Fig. 2. Iris image: (a) original image, (b) normalized image, and (c) normalized image with eyelid masking.

between the iris and the sclera) in the original gray-scale image $f_{org}(m_1, m_2)$ shown in Figure 2 (a). We use an ellipse as a model of the inner boundary. Let (l_1, l_2) be the lengths of the two principal axes of the ellipse, (c_1, c_2) be its center, and θ be the rotation angle. We can find the optimal estimate $(l_1, l_2, c_1, c_2, \theta)$ for the inner boundary by maximizing the following absolute difference:

$$|S(l_1 + \Delta l_1, l_2 + \Delta l_2, c_1, c_2, \theta) - S(l_1, l_2, c_1, c_2, \theta)|\,. \quad (1)$$

Here, Δl_1 and Δl_2 are small constants, and S is the N-point contour summation of pixel values along the ellipse:

$$S(l_1, l_2, c_1, c_2, \theta) = \sum_{n=0}^{N-1} f_{org}(p_1(n), p_2(n)), \quad (2)$$

where $p_1(n) = l_1 \cos\theta \cdot \cos(\frac{2\pi}{N-1}n) - l_2 \sin\theta \cdot \sin(\frac{2\pi}{N-1}n) + c_1$ and $p_2(n) = l_1 \sin\theta \cdot \cos(\frac{2\pi}{N-1}n) + l_2 \cos\theta \cdot \sin(\frac{2\pi}{N-1}n) + c_2$. Thus, we will detect the inner boundary as the ellipse on the image for which there will be sudden change in luminance summed around its perimeter. To reduce computation time, the parameter set $(l_1, l_2, c_1, c_2, \theta)$ can be simplified depending on iris images. In our experiments using the CASIA iris image database, assuming $\theta = 0$ causes no degradation on its performance. The outer boundary is detected in a similar manner.

B. Iris Normalization

Next step is to normalize iris to compensate for the elastic deformation in iris texture. We unwrap the iris region to a normalized rectangular block of a fixed size (256×128 pixels in our experiments). In order to remove the iris region occluded by the upper eyelid and eyelashes, we use only the lower half of the iris region (Figure 2 (a)) and apply a polar coordinate transformation (with its origin at the center of pupil) to obtain the normalized image shown in Figure 2 (b), where n_1 axis corresponds to the angle of polar coordinate system and n_2 axis corresponds to the radius.

In the transformed iris image, the irrelevant eyelid region should be masked as shown in Figure 2 (c). In general, the eyelid boundary can be modeled as an ellipse contour. Hence the same method to detect the inner boundary can be applied to eyelid detection.

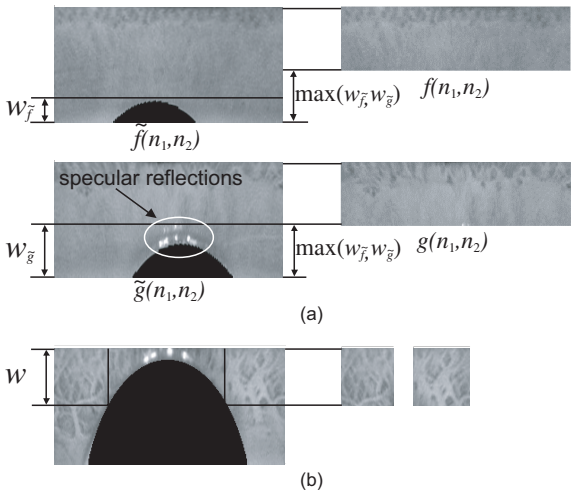

Fig. 3. Effective region extraction: (a) normal case, and (b) case when multiple sub-regions should be extracted.

III. Matching

This section describes the detailed process of effective region extraction, image alignment and matching score calculation. The key idea is to use phase-based image matching for image alignment and matching score calculation.

A. Effective Region Extraction

Given a pair of normalized iris images $\tilde{f}(n_1, n_2)$ and $\tilde{g}(n_1, n_2)$ to be compared, the purpose of this process is to extract, from the two images, the effective regions $f(n_1, n_2)$ and $g(n_1, n_2)$ of the same size, which do not contain irrelevant regions as illustrated in Figure 3 (a).

A problem occurs when the extracted effective region becomes too small to perform image matching. In such a case, we extract multiple effective sub-regions from each iris image as illustrated in Figure 3 (b) by changing the width parameter w. In our experiments, we extract 6 sub-regions from a single iris image by changing the parameter w as 55, 75 and 95 pixels.

B. Phase-Based Image Matching

Before discussing the image alignment and the matching score calculation, we introduce the principle of phase-based image matching using Phase-Only Correlation (POC) function [5]. Consider two $N_1 \times N_2$-pixel images, $f(n_1, n_2)$ and $g(n_1, n_2)$, where we assume that the index ranges are $n_1 = -M_1 \cdots M_1$ ($M_1 > 0$) and $n_2 = -M_2 \cdots M_2$ ($M_2 > 0$) for mathematical simplicity, and hence $N_1 = 2M_1 + 1$ and $N_2 = 2M_2 + 1$. Let $F(k_1, k_2)$ and $G(k_1, k_2)$ denote the 2D DFTs of the two images. $F(k_1, k_2)$ is given by

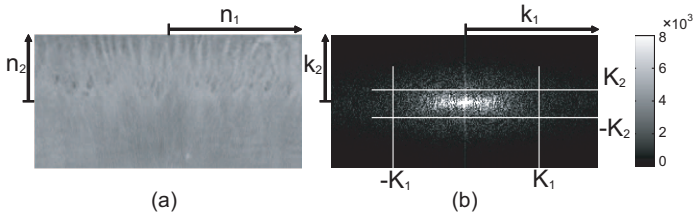

Fig. 4. Normalized iris image in (a) spatial domain, and in (b) frequency domain (amplitude spectrum), where $K_1 = 0.55M_1$ and $K_2 = 0.2M_2$.

$$F(k_1,k_2) = \sum_{n_1,n_2} f(n_1,n_2) W_{N_1}^{k_1 n_1} W_{N_2}^{k_2 n_2} = A_F(k_1,k_2) e^{j\theta_F(k_1,k_2)}, \quad (3)$$

where $k_1 = -M_1 \cdots M_1$, $k_2 = -M_2 \cdots M_2$, $W_{N_1} = e^{-j\frac{2\pi}{N_1}}$, $W_{N_2} = e^{-j\frac{2\pi}{N_2}}$, and $\sum_{n_1,n_2}$ denotes $\sum_{n_1=-M_1}^{M_1} \sum_{n_2=-M_2}^{M_2}$. $A_F(k_1,k_2)$ is amplitude and $\theta_F(k_1,k_2)$ is phase. $G(k_1,k_2)$ is defined in the same way. The cross-phase spectrum $R_{FG}(k_1,k_2)$ is given by

$$R_{FG}(k_1,k_2) = \frac{F(k_1,k_2)\overline{G(k_1,k_2)}}{|F(k_1,k_2)\overline{G(k_1,k_2)}|} = e^{j\theta(k_1,k_2)}, \quad (4)$$

where $\overline{G(k_1,k_2)}$ is the complex conjugate of $G(k_1,k_2)$ and $\theta(k_1,k_2)$ denotes the phase difference $\theta_F(k_1,k_2) - \theta_G(k_1,k_2)$. The POC function $r_{fg}(n_1,n_2)$ is the 2D Inverse DFT (2D IDFT) of $R_{FG}(k_1,k_2)$ and is given by

$$r_{fg}(n_1,n_2) = \frac{1}{N_1 N_2} \sum_{k_1,k_2} R_{FG}(k_1,k_2) W_{N_1}^{-k_1 n_1} W_{N_2}^{-k_2 n_2}, \quad (5)$$

where $\sum_{k_1,k_2}$ denotes $\sum_{k_1=-M_1}^{M_1} \sum_{k_2=-M_2}^{M_2}$. When two images are similar, their POC function gives a distinct sharp peak. When two images are not similar, the peak drops significantly. The height of the peak gives a good similarity measure for image matching, and the location of the peak shows the translational displacement between the images.

In our previous work [5], we have proposed the idea of BLPOC (Band-Limited Phase-Only Correlation) function for efficient matching of fingerprint images considering the inherent frequency components in fingerprint images. We have found that the same idea is also very effective for iris recognition. Our observation shows that (i) the 2D DFT of a normalized iris image contains meaningless phase components in high frequency domain, and that (ii) the effective frequency band of the normalized iris image is wider in k_1 direction than in k_2 direction (see Figure 4). The original POC function $r_{fg}(n_1,n_2)$ emphasizes the high frequency components, which may have less reliability. We observe that this reduces the height of the correlation peak significantly even if the given two iris images

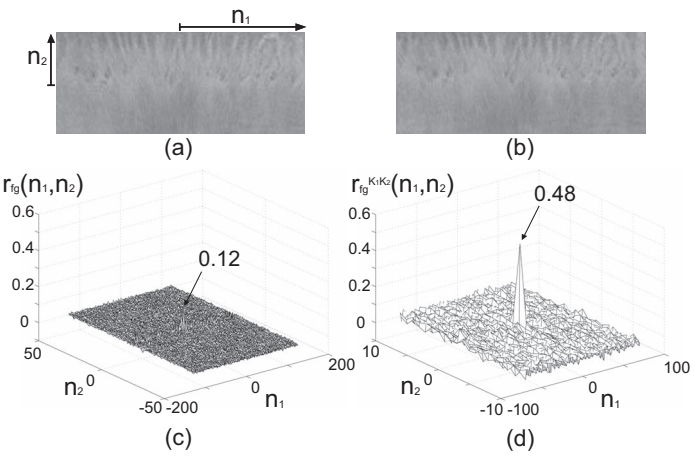

Fig. 5. Example of genuine matching using the original POC function and the BLPOC function: (a) iris image $f(n_1,n_2)$, (b) iris image $g(n_1,n_2)$, (c) original POC function $r_{fg}(n_1,n_2)$, and (d) BLPOC function $r_{fg}^{K_1K_2}(n_1,n_2)$.

are captured from a common eye. On the other hand, BLPOC function allows us to evaluate the similarity using the inherent frequency band within iris textures.

Assume that the ranges of the significant frequency band are given by $k_1 = -K_1 \cdots K_1$ and $k_2 = -K_2 \cdots K_2$, where $0 \le K_1 \le M_1$ and $0 \le K_2 \le M_2$ as shown in Figure 4 (b). Thus, the effective size of frequency spectrum is given by $L_1 = 2K_1 + 1$ and $L_2 = 2K_2 + 1$. The BLPOC function is given by

$$r_{fg}^{K_1K_2}(n_1,n_2) = \frac{1}{L_1 L_2} {\sum_{k_1,k_2}}' R_{FG}(k_1,k_2) W_{L_1}^{-k_1 n_1} W_{L_2}^{-k_2 n_2}, \quad (6)$$

where $n_1 = -K_1 \cdots K_1$, $n_2 = -K_2 \cdots K_2$, and $\sum'_{k_1,k_2}$ denotes $\sum_{k_1=-K_1}^{K_1} \sum_{k_2=-K_2}^{K_2}$. Note that the maximum value of the correlation peak of the BLPOC function is always normalized to 1 and does not depend on L_1 and L_2. Figure 5 shows an example of genuine matching using the original POC function r_{fg} and the BLPOC function $r_{fg}^{K_1K_2}$. The BLPOC function provides better discrimination capability than that of the original POC function.

C. Displacement Alignment

This step is to align the translational displacement between the extracted images (Figure 3). Rotation of the camera, head tilt and rotation of the eye within the eye socket may cause the displacements in normalized images. The displacement parameters can be obtained as the peak location of the POC function $r_{fg}(n_1,n_2)$. The obtained parameters are used to align the images.

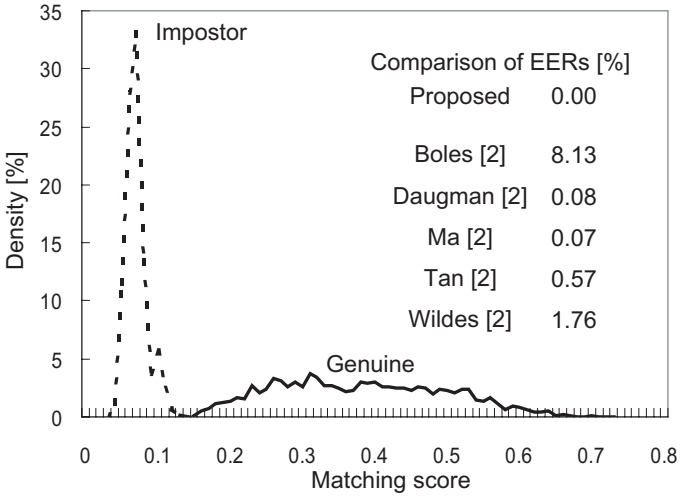

Fig. 6. Distributions of matching scores.

D. Matching Score Calculation

In this step, we calculate the BLPOC function $r_{fg}^{K_1 K_2}(n_1, n_2)$ between the aligned images $f(n_1, n_2)$ and $g(n_1, n_2)$, and evaluate the matching score. In the case of genuine matching, if the displacement between the two images is aligned, the correlation peak of the BLPOC function should appear at the origin $(n_1, n_2) = (0, 0)$. So, we calculate the matching score as the maximum peak value of the BLPOC function within the $r \times r$ window centered at the origin ($r = 11$ in our experiments). When multiple sub-regions are extracted as illustrated Figure 3 (b), the matching score is calculated by taking an average for effective sub-regions.

If the matching score is close to the threshold value to separate genuines and impostors, we calculate the matching score with scale correction (see Figure 1).

IV. Experiments and Discussions

This section describes a set of experiments using the CASIA iris image database (ver 1.0) [7] for evaluating matching performance. This database contains 756 gray-scale eye images (320×280 pixels) with 108 unique eyes and 7 different images of each unique eye. We first evaluate the genuine (intra-class) matching scores for all the possible combinations of genuine attempts (${}_7C_2 \times 108 = 2268$ attempts). Next, we evaluate the impostor (inter-class) matching scores for ${}_{108}C_2 = 5778$ impostor attempts, where we take a single image for each eye and make all the possible combinations of impostor attempts. Figure 6 shows distributions of genuine and impostor matching scores. The figure shows a good separation of genuine and impostor matching scores, where the minimum genuine matching score is 0.1464, and the maximum impostor matching score is 0.1428. The score between these values can be chosen as a threshold to distinguish between the two classes. Thus, for this experiment, we can achieve EER=0%, where the EER (Equal Error Rate) is the error rate where the FNMR (False Non-Match Rate) and the FMR (False Match Rate) are equal. Some reported values of EER from [2] using the CASIA iris image database are also shown in the same figure for reference. Note that the experimental condition in [2] is not the same as our case, because the complete database used in [2] is not available at [7] due to the usage rights of iris images. The number of iris images in the database available at [7] is smaller than the complete database. The result demonstrates a potential possibility of phase-based image matching for creating an efficient iris recognition system.

V. Conclusion

In our previous work, we have developed actual fingerprint verification units [6] based on phase-based image matching. In this paper, we have demonstrated that the same approach can be highly effective also for iris recognition. The proposed approach will be useful for implementing a unified hardware/software engine for multimodal biometric system with iris and fingerprint recognition capability.

Acknowledgment

Portions of the research in this paper use the CASIA iris image database collected by Institute of Automation, Chinese Academy of Sciences.

References

[1] J. Daugman, "High confidence visual recognition of persons by a test of statistical independence," *IEEE Trans. Pattern Analy. Machine Intell.*, vol. 15, pp. 1148–1161, Nov. 1993.

[2] L. Ma, T. Tan, Y. Wang, and D. Zhang, "Efficient iris recognition by characterizing key local variations," *IEEE Trans. Image Processing*, vol. 13, no. 6, pp. 739–750, June 2004.

[3] C. D. Kuglin and D. C. Hines, "The phase correlation image alignment method," *Proc. Int. Conf. on Cybernetics and Society*, pp. 163–165, 1975.

[4] K. Takita, T. Aoki, Y. Sasaki, T. Higuchi, and K. Kobayashi, "High-accuracy subpixel image registration based on phase-only correlation," *IEICE Trans. Fundamentals*, vol. E86-A, no. 8, pp. 1925–1934, Aug. 2003.

[5] K. Ito, H. Nakajima, K. Kobayashi, T. Aoki, and T. Higuchi, "A fingerprint matching algorithm using phase-only correlation," *IEICE Trans. Fundamentals*, vol. E87-A, no. 3, pp. 682–691, Mar. 2004.

[6] http://www.aoki.ecei.tohoku.ac.jp/poc/

[7] http://www.sinobiometris.com